1st International Conference on Structural Integrity

A Comparative LCF Study of S960QL High Strength Steel and S355J2 Mild Steel

Tomasz Ślęzak[a]*, Lucjan Śnieżek[a]

[a]*Military University of Technology, Faculty of Mechanical Engineering, Insitute of Machine Design, 2 Kaliskiego St., 00-908 Warsaw, Poland*

Abstract

Nowadays high strength steels are gained increasing popularity for use in steel constructions and machinery components. Their fatigue properties, however, are not yet well characterized, especially in comparison with widespread conventional structural steel S355J2. In this study were conducted the assessment of use HSS steel in extremely loaded components with existing plastic strains. In order to obtain the necessary characteristics and fatigue properties, materials were tested under LCF strain-based mode with strain ratio $R_\varepsilon = 0,1$ and strain rate of 10^{-2} 1/s. Because of its higher strength, S960QL steel exhibits a slightly higher fatigue resistant under the total strain amplitude lower than 0,5% compared to mild steel and similar under higher strains. Obtained results show that investigated HSS steel can successfully supersede presently used conventional mild steel in heavily loaded components simultaneously decreasing dead weight of the structure.

1. Introduction

With the increase of requirements concerning economic efficiency in production, operation and service of the building structures, installations and machines there are being developed new grades of structural materials. High consumption of structural materials in civil engineering and industry of machinery manufacturing together with production costs and limitations induced by environmental protection factors are causing that steels are the material

---

* Corresponding author. Tel.: +48-261-837-685; fax: +48-261-837-899.
  E-mail address: tomasz.slezak@wat.edu.pl

being evaluated for the purpose of reducing the weight of components. This aim is gained using steel products with smaller cross section or thickness what is countervailed by higher strength properties. Finally, it results in lower manufacturing costs and improvement of the operational characteristics like payload, lifting capacity and energy efficiency.

Nomenclature

A	percentage elongation after fracture
E	Young's modulus (modulus of elasticity)
K'	cyclic strength coefficient
N	number of cycles
N_f	number of cycles to failure (fatigue life)
R_m	ultimate tensile strength
$R_{p0,2}$	yield strength
Z	percentage reduction of area
b	fatigue strength exponent
c	fatigue ductility exponent
n'	cyclic strain hardening exponent
ε_f'	fatigue ductility coefficient
σ_f'	fatigue strength coefficient

Subscripts:

a	amplitude
ac	total amplitude
ae	amplitude of elastic component
ap	amplitude of plastic component

In order to meet above described demands two main groups of steels can be distinguished. Advanced high strength steels (AHSS) obtained in production process by controlled cooling followed by lower-temperature austenite transformation make the first the group. Final properties and microstructure of AHSS are depended on the percentage content of different microalloy elements and cooling process. Structure of dual phase (DP) steels consists of ferrite and martensite. In this case the strength properties are dependent on the percentage of martensite and the strength increases with increasing proportion of the martensite phase. Unique ductility during forming is imparted by appropriate grain size of ferrite. Complex phase (CP) steels have extreme refined multiphase microstructure containing ferrite/bainite matrix with small volume of martensite, pearlite and retained austenite. The grain refinement is created by precipitation of microalloying elements like Ti, Nb or V and retarded recrystallization. This results in high value of yield strength to tensile strength ratio what creates excellent susceptibility to cold forming, stretch forming and roll forming. Transformation-induced plasticity (TRIP) steels consists of a primary ferrite matrix with minimum five percentage of retained austenite and the dispersions of bainite and martensite in varying amounts. Retained austenite has crucial influence on the strength properties of TRIP steels. During plastic deformation in manufacturing or in service the retained austenite progressively transforms to martensite within the increase of strain [2,7]. This phenomenon is named as TRIP effect.

Second group of steels includes the grades of High Performance Steels (HPS). There are two main grades of steels, namely High Strength Low Alloyed (HSLA) and High Strength Steels (HSS). They are fabricated in two basic processes: thermo-mechanical processing techniques (TMCP) and liquid-quenching and tempering (Q&T) process. A major feature of these grades is low level of carbon and the addictions of micro alloying elements resulting in low value of Carbon Equivalent (CE) and improved weldability [3,4]. A structure is ultra fine-grained and consists of tempered martensite and bainite, both lower and upper induced by controlled rolling with subcooling and structure refining elements, e.g. Ti, V or Al. Strength properties are controlled by the proportion of martensite and bainite. The yield strength and ultimate tensile strength grow within increasing percentage of martensite [1,3].

The purpose of this study is to perform experimental investigation of the fatigue properties S960QL high strength steel and to compare with the results obtained for S355J2 structural mild steel. The fatigue behavior was evaluated through low cycle fatigue tests (LCF) of smooth and small size specimens. The fatigue tests were carried out under sinusoidal strain-controlled mode with positive strain asymmetry rate and constant average value of strain rate. Obtained surfaces of fatigue fractures were carefully investigated in order to perform detail description of the mechanisms of crack initiation, indicating the origins and the nature of fatigue crack growth.

2. Experimental investigation

2.1. Investigated materials

Fatigue tests were carried out on two grades of structural steels, namely the high strength steel S960QL and S355J2 mild steel. Chemical composition and mechanical properties are shown in Table 1 and Table 2, respectively.

Table 1. Chemical composition of examined steels Wt[%].

	C	Si	Mn	Cr	Mo	Ni	Al	V	Cu
S960QL	0,18	0,36	1,19	0,23	0,66	0,06	0,11	0,03	0,19
S355J2	0,17	0,04	1,54	0,02	-	0,04	0,07	-	0,08

Measurements of chemical composition were performed with the use of SEM equipped with EDS spectrometer. Using this method it is limited to measure a quantity of carbon thus the values placed in Table 1 as obtained by a measurement correspond to the value from certificate.

Table 2. Mechanical properties of examined steels.

	E (MPa)	$R_{p0,2}$ (MPa)	R_m (MPa)	A (%)	Z (%)
S960QL	$2,20 \times 10^5$	974	1070	14,2	45,6
S355J2	$1,92 \times 10^5$	385	531	30,7	64,4

Strength properties were determined in tensile tests conducted according to ISO 6892-1 [9]. Some discrepancies were revealed, nevertheless experimental results show that minimum strength properties are fulfilled.

The high strength steel S960QL is obtained in production process of quenching and tempering with controlled rolling. The microstructure is shown in Fig. 1a. This steel is characterized by fine-grained martensite-bainitic structure with a grain size of 5-25 μm. Addiction of vanadium affects the permanent carbides locking grain growth.

The mild steel S355J2 is produced by hot rolling and investigated material was delivered in normalized state. Microstructure is shown in Fig. 1b. This structure is characteristic for non alloy carbon steels and consists of grains of ferrite (F) and pearlite (P). In comparison with S960QL the band texture is clearly visible.
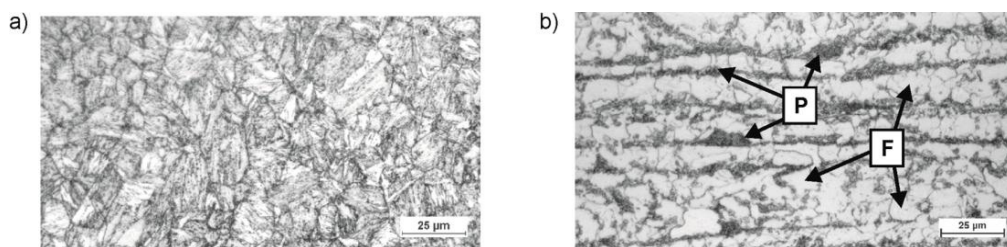

Fig. 1. Microstructure of S960QL HSS steel (a) and S355J2 mild steel; F - ferrite, P - pearlite.

2.2. Specimen, test equipment and procedure

The test specimens were cut from sheets ordered for this study with nominal thickness of 6 mm. The low cycle fatigue tests (LCF) were conducted using flat-sheet fatigue specimen with rectangular cross section prepared in accordance with ASTM standard E606-4 [8] with dimensions shown in Fig. 2. In order to make the tests more adequate in comparison with real application the surface of specimens was not machined and they were tested in delivery state. This approach takes into account the influence of specific surface conditions and imperfections on fatigue life.
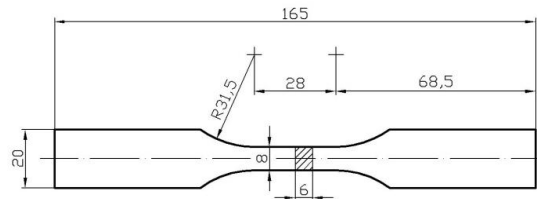
Fig. 2. Dimensions of specimen used in LCF tests.

The tests were conducted with the use of servohydraulic test system Instron 8802 equipped with the dynamic extensometer of a 25mm gauge length. This system is capable to exert as much as 250kN force in tension which is sufficient in our investigation. Instron 8802 has digital control system which provides all the signals necessary to control fatigue tests through the digital closed-loop mechanical servo system.

Fatigue tests were carried out at room temperature under strain-controlled mode where the loading was defined by the maximum value of total strain amplitude ε_a under sinusoidal mode of load. There were assumed constant values of strain ratio $R_\varepsilon = 0,1$ and strain rate (average value) of 10^{-2} s^{-1}. Intended value of strain ratio is due to prevent specimens against heat development under greater strain amplitudes and to shorten the duration of tests under lower. LCF tests were conducted under fife levels of ε_a, namely 0,3%, 0,4%, 0,5%, 0,75% and 1,0%. The failure criterion was defined by the drop of maximum force (stress). The fatigue life N_f equals the cycle number at which the maximum force decreases by 25% because of a crack or crack being present in comparison with the maximum force in the first cycle. All the data obtained from the tests were recorded by a computer software and could be monitored during testing.

3. Experimental results

It should be emphatically noted that results are obtained for specimens tested not for strain ratio $R_\varepsilon = -1$, what is usually assumed, but under value of 0,1. In this conditions material is extremely loaded with stresses being far above a yield strength (a maximum strain reaches up to 2,2%) even under low value of strain amplitude.

3.1. Failure analysis

Exemplary hysteresis loops obtained for both examined steels are shown in Fig. 3. Each graph presents fife representative stress-strain curves: first quarter-cycle with succeeding first full cycle $N=1$ (black), the tenth cycle $N=10$ (red), stabilized hysteresis loop corresponding $N=N_f/2$ (orange), hysteresis loops corresponding 10% decrease of maximum force $N_{90\%}$ (green), often defined as the point of crack initiation and last cycle for N_f (blue line). Graphs shown in Fig. 4 present the changes of maximum stress σ_{max} and stress amplitude σ_a obtained under different levels of loading ε_{ac}.

On the basis of shapes presented hysteresis loops it can be easily seen that the areas of loops for mild steel are greater than for HSS steel. It means that S355J2 steel is more sensitive to plastic strains and has to dissipate more energy in single cycle in comparison with S960QL. It results mainly from the structure – ferrite-pearlitic is characterized by higher plasticity and thus lower strength. Moreover, the percentage drop of maximum stress is faster and more visible in the case of mild steel and heavily loaded HSS steel what is indicated by relative position

of hysteresis $N_f/2$ and $N_{90\%}$. In the case of S960QL shown in Fig. 3a, the stresses had stabilized earlier and just after they have dropped during failure below the value of 90% initial stress.
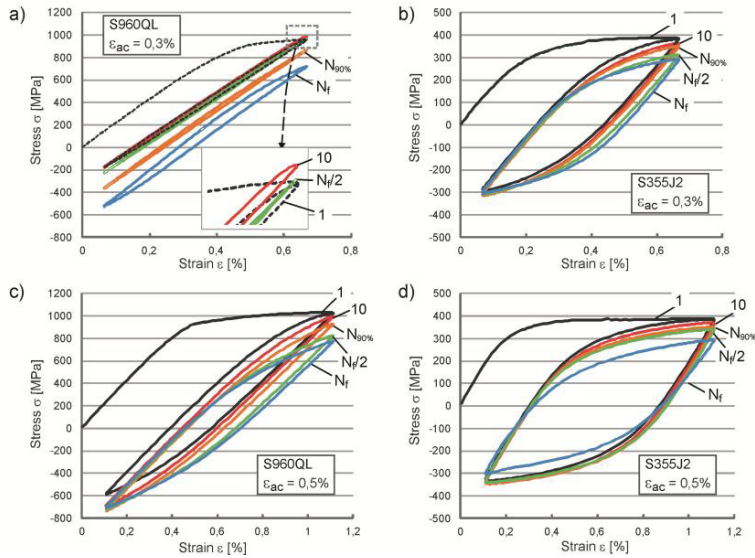

Fig. 3. Hysteresis loops obtained for S960QL (a,c) and S355J2 steel (b,d) examined under $\varepsilon_{ac} = 0,3\%$ (a,b) and $\varepsilon_{ac} = 0,5\%$ (c,d)

Results for S960QL steel are presented in Fig. 4a. There can be observed significant decrease of maximum stress σ_{max} before crack initiation comparing to mild steel (Fig. 4b). The decreases reached of about 25%, nevertheless, it was not noticed in specimen tested under $\varepsilon_{ac} = 0,3\%$. All courses for S355J2 steel (Fig. 4b) were similar and reached up to 10-20%. Moreover, initial σ_{max} for HSS steel tested under $\varepsilon_{ac} = 0,5$-$1,0\%$ were comparable while for mild steel increased, what was caused by their tensile characteristic.
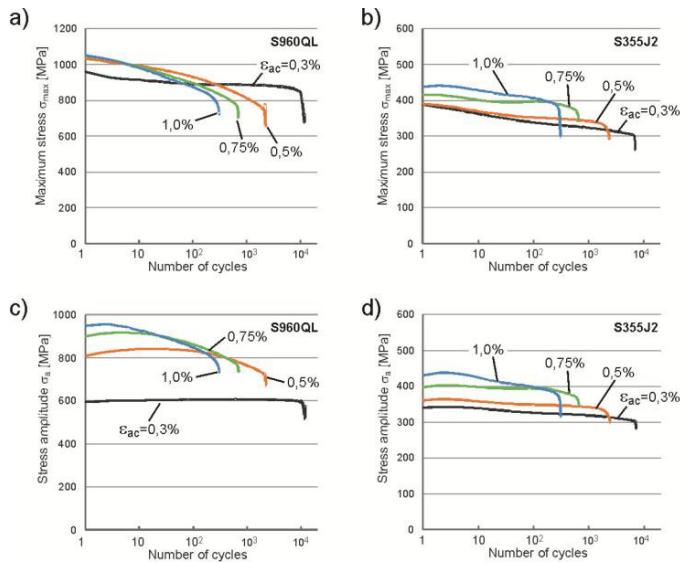

Fig. 4. Changes of maximum stress (a,b) and stress amplitude (c,d) obtained for S960QL (a,c) and S355J2 steel (b,d)

Greater drops were noticed also for stress amplitude σ_a (Fig. 4c) except of specimen tested under $\varepsilon_{ac} = 0,3\%$, where σ_a was almost constant. More stabilized declines were observed in all cases of mild steel specimens (Fig. 4d).

3.2. Cyclic stress-strain behavior of S960QL and S355J2 steels

Data recorded during LCF tests were used to determine cyclic properties of examined materials. Firstly, cyclic strength coefficient K' and cyclic strain hardening exponent n' were determined on the basis of parameters obtained from stabilized hysteresis loops. It was assumed that curves described by equation (1) are usually straight lines in double-logarithmic system $log\ \sigma_a$ - $log\ \varepsilon_{ap}$.

$$\sigma_a = K'\left(\varepsilon_{ap}\right)^{n'} \tag{1}$$

Determined values of coefficient and exponent make it possible to describe the cyclic stress–strain curve by means of constitutive Ramberg–Osgood equation (2).

$$\varepsilon = \frac{\sigma}{E} + \left(\frac{\sigma}{K'}\right)^{\frac{1}{n'}} \tag{2}$$

Received data were also used to perform fatigue analysis based on Manson-Coffin-Basquin relationship (3). Gained values of fatigue coefficients and exponents enable to express the strain-life curve are shown in Fig. 4. and in Table 3. Determined M-C-B dependences were placed on respective graphs.

$$\varepsilon_{ac} = \varepsilon_{ae} + \varepsilon_{ap} = \frac{\sigma_f'}{E} \cdot \left(2N_f\right)^b + \varepsilon_f' \cdot \left(2N_f\right)^c \tag{3}$$

On the basis of presented graphs we can notice that greater plastic strains, comparing to S960QL, were induced in S355J2 steel. It causes simultaneously lower contribution of elastic component in total strain in the case of mild steel and higher in HSS (red dashed line in Fig. 4). Moreover, both lines describing elastic and plastic component in HSS case with respect to mild steel intersect at lower number of reversals and higher value of strain amplitude in point named as a transition fatigue life. It means that fatigue of HSS steel is dominated almost in whole range of load ($\varepsilon_{ac} < 8,86 \cdot 10^{-3}$) by elastic component, when the range for mild steel is significantly lower ($\varepsilon_{ac} < 3,66 \cdot 10^{-3}$).

Table 3 presents the values of cyclic material properties and the coefficients and exponents used in Eq. (3).
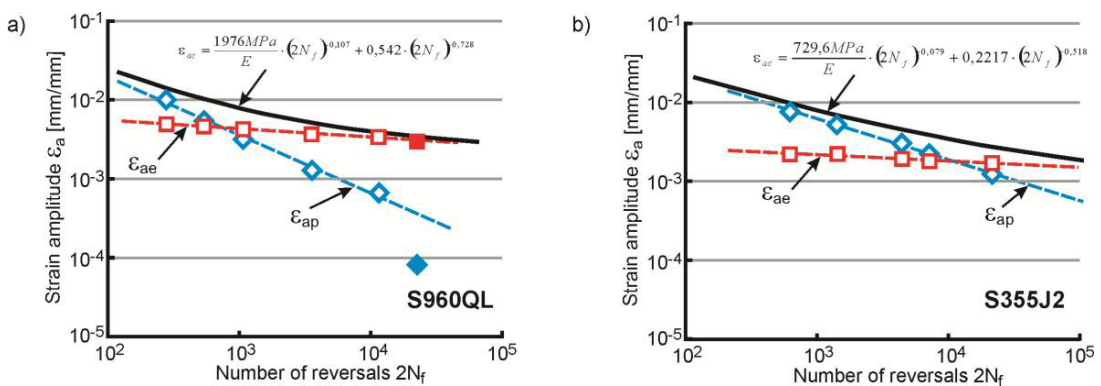

Fig. 5. Strain-life curves for S960QL (a) and S355J2 steel (b); full signs indicate data not considered

Table 3. Cyclic material properties of S960QL and S355J2 steels tested under $R_\varepsilon = 0,1$.

	K' (MPa)	n'	σ'_f (MPa)	ε'_f	b	c
S960QL	1236	0,0769	1976	0,5421	-0,107	-0,728
S355J2	818,9	0,1476	729,6	0,2217	-0,079	-0,518

Fatigue life N_f obtained for considered materials has shown some similarity. Nevertheless, conducted analysis of cyclic behavior of S960QL and S355J2 steels have revealed significant differences. Determined cyclic properties (Table 3) and strain-life curves (Fig. 5) unambiguously indicate that there have place essential factors connected with crack initiation and failure mechanisms.

3.3. Fractography investigation

Fatigue fracture pictures of specimens tested under $\varepsilon_{ac} = 0,4\%$ and made using SEM are presented in Fig. 6. Recognized fatigue zones (FZ) are surrounded by lines. In case of S96QL steel (Fig. 6a) fatigue area is characterized by irregularity with numerous surface origins. There have been propagating many individual local cracks which joined by downcasts to one main rupture. Other character was found for S355J2 steel (Fig. 6b). Fatigue area has regular shape, similar to semi-elliptical crack. There were revealed one major origin (MO) and few secondary.
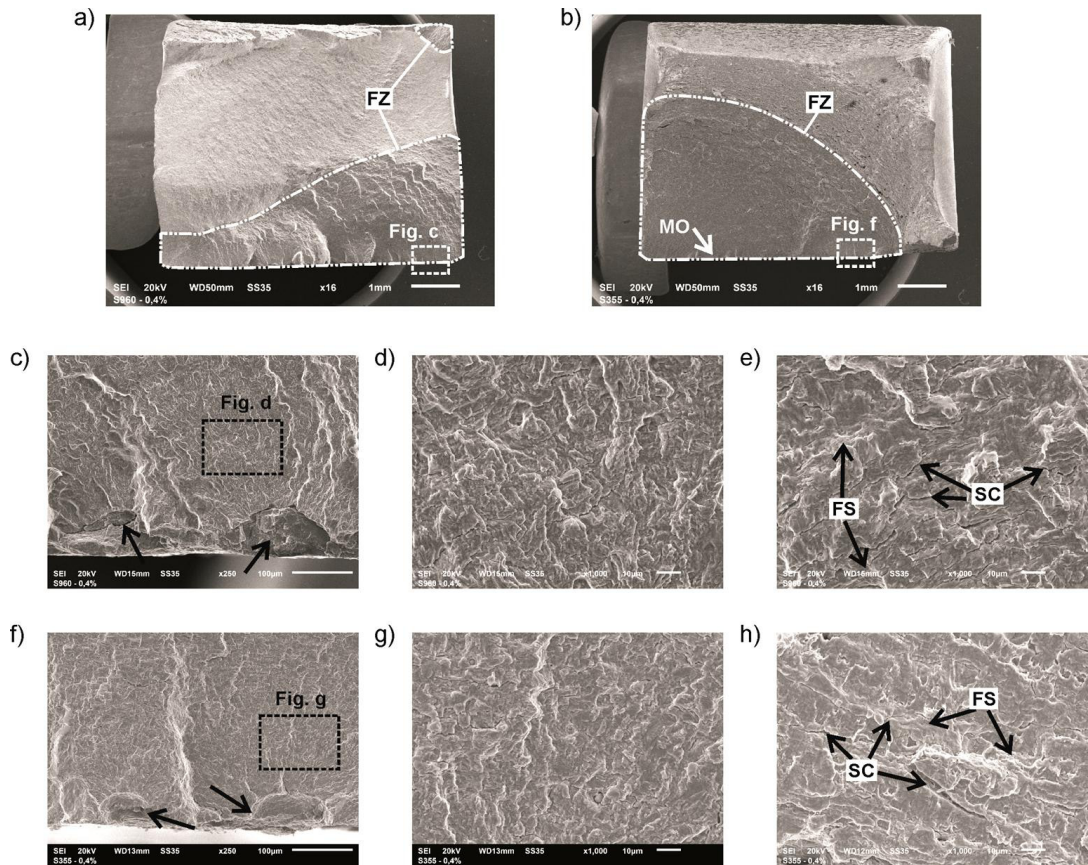

Fig. 6. Main differences in fatigue zone shape (a,b), crack initiation (c,f) and propagation (d,e,g,h) observed on the rupture surfaces of S960QL (a,c,d,e) and S355J2 (b,f,g,h) specimens tested under $\varepsilon_{ac} = 0,4\%$; detailed description in and explanation of marks in body text.

The exemplary origins for HSS and mild steel are shown in Fig 6c and f, respectively. Cracks in S960QL steel were initiated in several points by hard and brittle remains of rolled-in scale (Fig 6d). The same initiation mechanism was observed by authors in previous study concerning HSS steels [5,6]. Other nature of initiation was noticed in S355J2 steel. Local decohesion of material caused by plastic strains has resulted in semi-elliptical microcracks from which fatigue cracks have propagated (Fig. 6f). There can be clearly stated stages of initiation and stable propagation what is very difficult for HSS steel.

Initial stage of crack advance (~0,1 mm from the initiator) is shown in Figs. 6d and g. Ductile nature of cracking has been preserved in both tested materials. Nevertheless, in the case of S960QL steel the rupture surface is distinctly ragged. In the structure composed of very strength phases, eg. martensite, the crack are locally blocked and can be made to meander from frequent crack deflection what influences crack growth properties. Crack surface shown in Fig 6g is more regular, but some additionally impairing inclusions are noticeable. Figs. 6e,h present the stage of high crack growth rate (at the depth of ~0,5 mm). There is also preserved the ductile nature of cracking but the surface was seriously damaged by imposed strains causing high compressive stresses (in compress phase of the load). As a result can by noticed squashed fatigue striations (FS), flattened surface of rupture and numerous secondary cracks (SC).

4. Conclusions

A research program was initiated to compare the differences in fatigue behavior between two structural steels, namely S960QL high strength steel and S355J2 mild steel. Cyclic material properties were obtained from fatigue tests conducted under strain-based loading. The following conclusions can be stated from this study.

1. The HSS and mild steels have shown similar fatigue life under higher values of total strains amplitude, but the fatigue life under strains amplitude lower than 0,5% is greater for S960QL steel, what is very desirable.
2. The damage of investigated S960QL steel is dominated by elastic component of strains which is characterized by low value of strain energy dissipation in particular cycles and limited susceptibility to plastic strains.
3. The differences of the determined cyclic properties and fatigue behavior are reflected in failure mechanisms. The crack growth in S9060QL steel is blocked by high strength structural phases changing the direction of propagation where in mild steel the material has experienced serious ductile strains.

References

[1] J. Hildebrand, F. Werner, Change of structural condition of welded joints between high-strength fine-grained steels and structural steels, in: J Civ Eng Manag, Vol X, No. 2, Technika, Vilnius, 2004, pp. 87-95.
[2] X. Long, S.K. Khanna, Fatigue properties and failure characterization of spot welded high strength steel sheet, Int J Fatig 29 (2007) 879-886.
[3] P.K. Ray, R.I. Ganguly, A.K. Panda, Optimization of mechanical properties of an HSLA-100 steel through control of heat treatment variables, Mat Sci Eng A 346 (2003) 122–131.
[4] B.K. Show1, R. Veerababu, R. Balamuralikrishnan, G. Malakondaiah, Effect of vanadium and titanium modification on the microstructure and mechanical properties of a microalloyed HSLA steel, Mat Sci Eng A 527 (2010) 1595–1604.
[5] T. Ślęzak, L. Śnieżek, Fatigue Properties and Cracking of High Strength Steel S1100QL Welded Joints, Key Eng Mat Vol. 598 (2014), pp. 237-242
[6] T. Ślęzak, L. Śnieżek, K. Grzelak, Influence of the usage of the high-energy joining technology on the properties of welds in high strength steel, Proceedings of 9th International Conference ITELMS '2014, May 22-23, 2014, Panevėžys, Lithuania, pp. 221-226.
[7] C. Wang, H. Ding, M. Cai, B. Rolfe, Multi-phase microstructure design of a novel high strength TRIP steel through experimental methodology, Mat Sci Eng A 610 (2014) 436–444.
[8] ASTM E-606 Standard Test Method for Strain-Controlled Fatigue Testing
[9] ISO 6892-1: Metallic materials – Tensile testing – Part 1: Method of test at room temperature